Effect of High Ammonium Salt Concentration and Temperature on the Structure, Morphology, and Ionic Conductivity of Proton-Conductor Solid Polymer Electrolytes Based PVA

Maryam A. M. Saeed [1] and Omed Gh. Abdullah [2],*

[1] Department of Physics, College of Science, University of Mosul, Mosul 41002, Iraq; alhabishmeryem@gmail.com
[2] Advanced Materials Research Lab., Department of Physics, College of Science, University of Sulaimani, Sulaymaniyah, Kurdistan Region 46001, Iraq
*   Correspondence: omed.abdullah@univsul.edu.iq

Abstract: Polyvinyl alcohol (PVA) based proton-conducting solid polymer electrolyte was prepared with a high salt concentration of ammonium nitrate (NH_4NO_3) by the technique of solvent casting. From the X-ray diffraction studies, the semicrystalline nature of PVA with the inclusion of NH_4NO_3 was studied. XRD analysis indicates that the highest ion conductive sample exhibits the minimum crystalline nature. The decreasing trend of Jonscher-exponent with temperature rise reveals that the present system is insured by the correlated barrier hopping (CBH) model. The maximum room temperature conductivity was found to be 5.17×10^{-5} S/cm for PVA loaded 30 wt.% of NH_4NO_3. The ionic transport of the proton-conducting solid polymer electrolyte was studied at the temperature range of 303–353 K. The conductivity-temperature relationship of the systems was analyzed using both the Arrhenius and Vogel–Tammann–Fulcher (VTF) models to explain the ionic hopping mechanism for the system.

Keywords: proton conductor; polymer electrolyte; ionic conductivity; arrhenius; VTF; CBH

1. Introduction

Solid polymer electrolytes (SPEs) are crucial compounds having promising applications for electrochemical devices, such as high powered solid-state rechargeable batteries, supercapacitors, chemical sensors, electrochromic displays, and fuel cells due to several advantages over the gel and liquid electrolytes [1–4]. The principal advantages of SPEs are their good mechanical properties, adaptability, wide electrochemical accuracy, simplicity of manufacture thin films, and flexibility [5,6]. The SPEs are characterized as ionic conducting polymer materials that are sophisticated by dissolving appropriate salt in the high molecular weight polar polymers.

Over the past decades, SPEs incorporated with lithium salts are prepared excessively due to an abundance of lithium salts, small Li-ion radii, and being lightweight. They are systematically investigated to reveal the possibility of making lithium-ion rechargeable batteries with high specific capacity and high electrochemical reduction potential [7]. Nowadays, proton-conducting SPEs have gained more attention due to their extensive applications in electrochemical sensors, reactors, and proton-exchange membrane fuel cells [8,9]. A literature survey reveals that incorporating ammonium salts into polar polymer produces proton-conducting electrolyte, due to one loosely bound of four protons attached to nitrogen [8,10].

Many researchers have already studied proton-conducting SPEs by incorporating ammonium salts to different polar polymers such as polyvinyl pyrrolidone, polyethylene oxide, polyvinyl alcohol, polyvinyl chloride, and polyacrylonitrile [11–13]. From the literature study, polyvinyl alcohol (PVA) has attracted great attention due to its good film-forming, good mechanical strength, biocompatibility, biodegradability, and nontoxicity [14,15]. PVA is a hydrophilic, synthetic, dielectric, semicrystalline polymer material at room temperature, which is widely used as a host matrix in the various SPE systems due to its durable polar nature [5,16]. The electrical conductivity of PVA was enhanced by some researchers upon the addition of different ammonium salts to prepare proton (H^+)-conducting SPEs. Radha et al. [17] reported the highest ionic conductivity at ambient temperature in the order of 10^{-6} S/cm for PVA/NH_4F proton-conducting SPEs. Hema et al. [18] reported the enhancement in ionic conductivity value in the order of 10^{-3} S/cm for PVA/NH_4I, 10^{-4} S/cm for PVA/NH_4Br, and 10^{-5} S/cm for PVA/NH_4Cl proton-conducting SPEs. In this work, series of proton-conducting SPEs are prepared from PVA as the host matrix, and the low-cost ammonium nitrate (NH_4NO_3) is used as a proton source for improving the ionic conductivity of the system. The structural, electrical, and transport properties of the prepared samples are studied as a function of salt concentrations, frequency, and temperature to expect the possible applications of the system.

2. Materials and Methods

Polyvinyl alcohol (PVA), low molecular weight, 98–99% hydrolyzed, purchased from Alfa Aesar (Kandel, Germany), and ammonium nitrate (NH_4NO_3), Mw = 80.04 g/mol, purchased from Merck (Darmstadt, Germany), were used as raw materials. Double-distilled water was used as a solvent in the experiment.

To set up a series of high salt concentration proton-conducting SPE films loaded with 10, 20, 30, 40, and 50 wt.% of NH_4NO_3, 2 g of PVA was dissolved in 40 mL double-distilled water separately, and the appropriate amount of salts dissolved in 5 mL were mixed together under stirring at room temperature until viscous homogeneous mixtures were achieved. The final polymer solution was cast in PP Petri dishes and dried slowly at the ambient temperature for the films to form. Since PVA has a hydrophilic nature, to ensure dryness of the films, the samples were kept in a dust-free chamber with silica gel for 14 days before being used in experiments. The flat, coherent films had been achieved and set aside in desiccators prior to characterization. The proton-conducting SPE films were coded as SPE-10, SPE-20, SPE-30, SPE-40, and SPE-50, for PVA incorporated, respectively, with 10, 20, 30, 40, and 50 wt.% of NH_4NO_3 salt.

Structural behavior of the prepared proton-conducting SPEs are characterized by X-ray diffractometer made by Bruker D8 (Karlsruhe, Germany) with Cu-Kα radiation (λ = 1.5418 Å) with an increment of 0.02° in the range of 10°–70°. The change in surface morphologies of the prepared films was examined using JEOL JSM-6060 scanning electron microscopy (SEM (Tokyo, Japan)) at an accelerating voltage of 20 kV. Prior to imaging, all samples were coated with a thin gold layer by a sputtering process. Impedance spectroscopy analysis was carried out using KEYSIGHT E4980A LCR Meter (Santa Rosa, CA, USA) within a frequency range of 100 Hz–2 MHz in the temperature range of 303–353 K.

3. Results and Discussion

3.1. X-ray Diffraction Studies

The structural properties of pure PVA and PVA/NH_4NO_3 proton-conducting SPE films were evaluated utilizing X-ray diffraction (XRD) studies and depicted in Figure 1. In the case of pure PVA, a broad, intense peak observed at a scattering angle centered at 2θ = 19.25°, indicate the semicrystalline structure of PVA [19,20]. The occurrence of the semicrystalline structure of PVA mainly arose due to a strong intramolecular and intermolecular hydrogen bonding between PVA molecules [21]. The intensity of the characterized peak of PVA was gradually decreased with increasing salt content and disappeared

at high salt concentrations, which implies the changes that occurred in the semicrystalline phase of the PVA matrix, due to the interaction between hydroxyl groups of the PVA and cations of the dissolved salt [22,23].
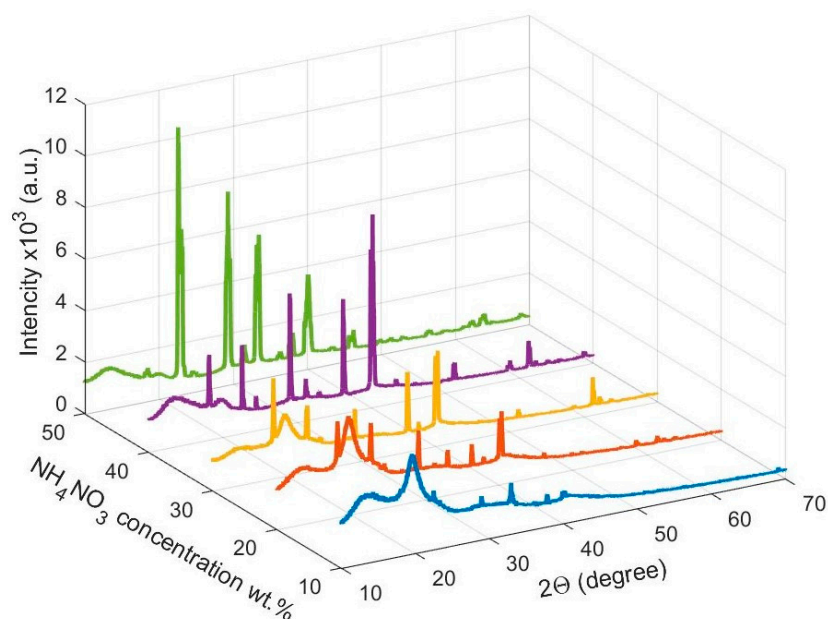

Figure 1. XRD pattern plots for PVA/NH$_4$NO$_3$ proton-conducting SPE films.

The PVA/NH$_4$NO$_3$ proton-conducting SPE films show some sharp diffraction peaks, which depict the crystalline structure of NH$_3$NO$_3$ according to the Joint Committee on Powder Diffraction Standards (JCPDS) card No. 83-0520. [24]. This indicates the presence of some undissociated NH$_4$NO$_3$ salt due to the high salt concentration in the present proton-conducting SPE samples. The increase in the relative intensity of the characteristic peaks of NH$_3$NO$_3$ in the SPEs with increasing salt concentration was attributed to ion association and salt aggregation at the surface of the film, as described by Shuhaimi et al. [25]. A relationship between the intensity of the XRD peaks and the crystallinity has been reported by numerous researchers [26,27]. The percentage of crystallinity (χ_c) was calculated from the following relationship [28,29];

$$\chi_c = \frac{A_c}{A_t} \times 100\% \tag{1}$$

where A_c and A_t are the area under the crystalline peaks and the total area of the diffractogram, respectively, which were determined from the deconvolution of the XRD spectra using Fityk software [30]. The XRD pattern was fitted by Gaussian function mode. The deconvolution of the XRD peaks for pure PVA and PVA/NH$_4$NO$_3$ proton-conducting SPE films shown in Figure 2 and the calculated value of χ_c is displayed in Table 1. The outer graphs in Figure 2 show the deconvoluted peaks for both the crystalline and amorphous regions, which was used to determine A_t, whereas, the inner graph depicts only the crystalline peaks, which was used to calculate A_c. It can also be observed that the hump of pure PVA spectrum is deconvoluted into four peaks, whereas the XRD spectra of SPEs were deconvoluted into 10–14 peaks, depending on the number of crystalline peaks appearing in the XRD pattern, in order to obtain a more accurate estimate of the crystallinity percentage of the system.
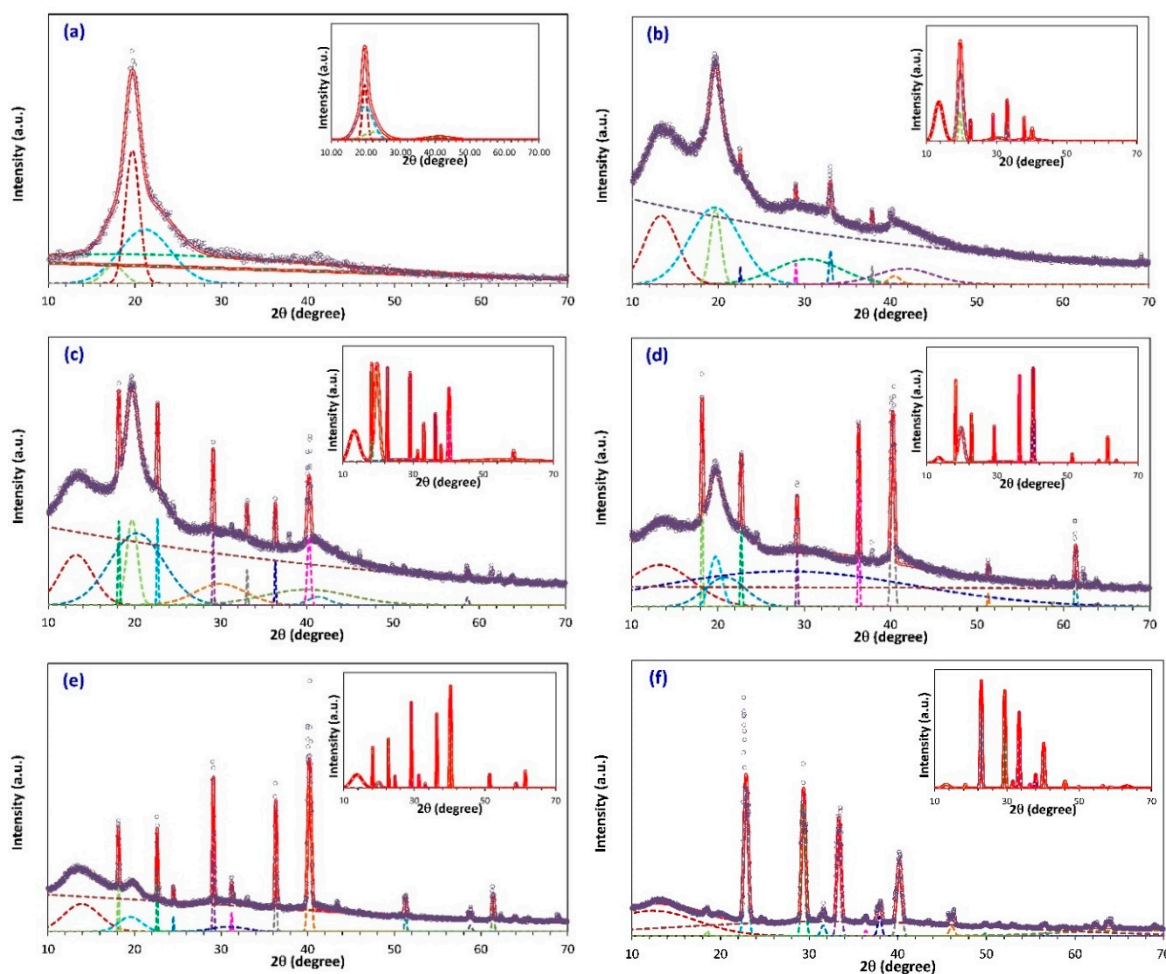
Figure 2. Represented the deconvoluted XRD peaks for (**a**) pure PVA, (**b**) SPE-10, (**c**) SPE-20, (**d**) SPE-30, (**e**) SPE-40, (**f**) SPE-50. The graphs show the peaks for both the crystalline and amorphous regions. The inner graph depicts the crystalline peaks only. (The solid lines represent the sum of the Gaussian fits in dotted lines).

Table 1. Crystalline, total area, and degree of crystallinity (χ_c for pure PVA and PVA/NH$_4$NO$_3$ proton-conducting SPE films.

Samples	A_c	A_t	χ_c
Pure PVA	9734.15	24,827.16	39.20
SPE-10	4864.19	27,295.78	17.82
SPE-20	7320.78	65,735.29	11.13
SPE-30	5410.93	54,434.50	9.94
SPE-40	7433.04	53,423.04	13.91
SPE-50	13,342.05	61,947.55	21.53

It can be inferred from Table 1 that the sample containing 30 wt.% NH$_4$NO$_3$ exhibits the minimum degree of crystallinity (highest amorphous nature). It has been well reported that the ionic conductivity of SPEs increases with the increase in the amorphous domains [31,32]. Thus, it can be predicted that the proton-conducting SPE sample containing 30 wt.% NH$_4$NO$_3$ exhibits the highest electrical conductivity at room temperature.

3.2. Morphological Study

The surface morphology images for the prepared PVA/NH_4NO_3 SPE films with different salt contents are shown in Figure 3. The sample with low salt concentrations shows almost smooth and homogeneous surface morphology, while the much rougher surface texture was perceived for the high salt concentration sample (SPE-50). It is well reported in the literature that the enhanced surface roughness of the SPEs at high salt concentration mainly occurs due to the salt aggregation out of the surface [33,34]. Thus, at high salt content, the dissociated ion pairs begin to recombine to form a neutral salt and then salt aggregations out of the surface of the SPEs. Kadir et al. [35] also reported a similar observation for chitosan-polyethylene oxide doped NH_4NO_3.
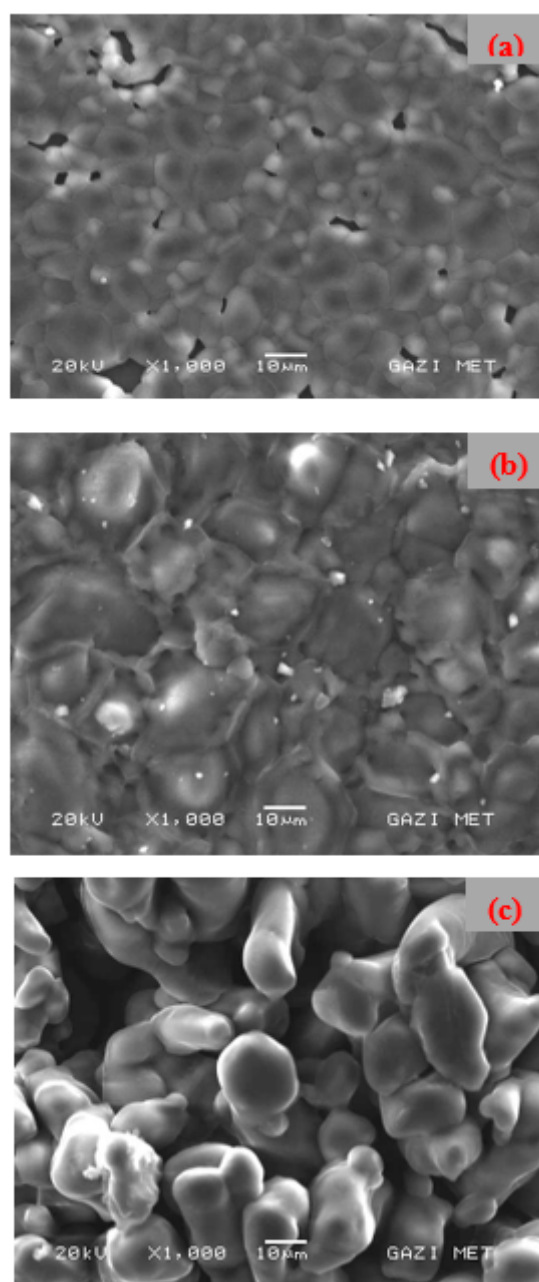

Figure 3. SEM micrographs of SPEs with different salt concentrations: (**a**) SPE-10, (**b**) SPE-30, and (**c**) SPE-50.

According to the previous reports [36,37], the conducting ions move more freely in the electrolyte with smoother surface morphology and therefore caused an overall enhancement in conductivity of SPEs. Some researchers successfully established a correlation between surface roughness and DC conductivity [33,36]. They conclude that the crystalline aggregations of undissolved salt out of the film surface at high salt content caused a significant decrease in the number of charge carriers, and hence lead to the reduction in DC conductivity of the system [38].

3.3. Electrical Conductivity Studies

3.3.1. Cole-Cole Plot

Figure 4 shows the relation of the real part (Z') and the imaginary part (Z'') of complex impedance for pure PVA and PVA/NH$_4$NO$_3$ proton-conducting SPE films with different concentration of NH$_4$NO$_3$ at two temperatures, 303 and 353 K. The Cole-Cole plots for PVA/NH$_4$NO$_3$ proton-conducting SPE films showed one semicircle arc that is followed by a spike at high temperature, which indicates a parallel combination of resistance and a capacitance in series [39]. Monitoring of a single semicircular arc for all SPEs is an indication of only one type of relaxation strategy existing in this system [40]. The intercept of the semicircle arc in the Cole-Cole plot with the real axis at the lower frequency end is usually used to determine the bulk resistance of SPE.
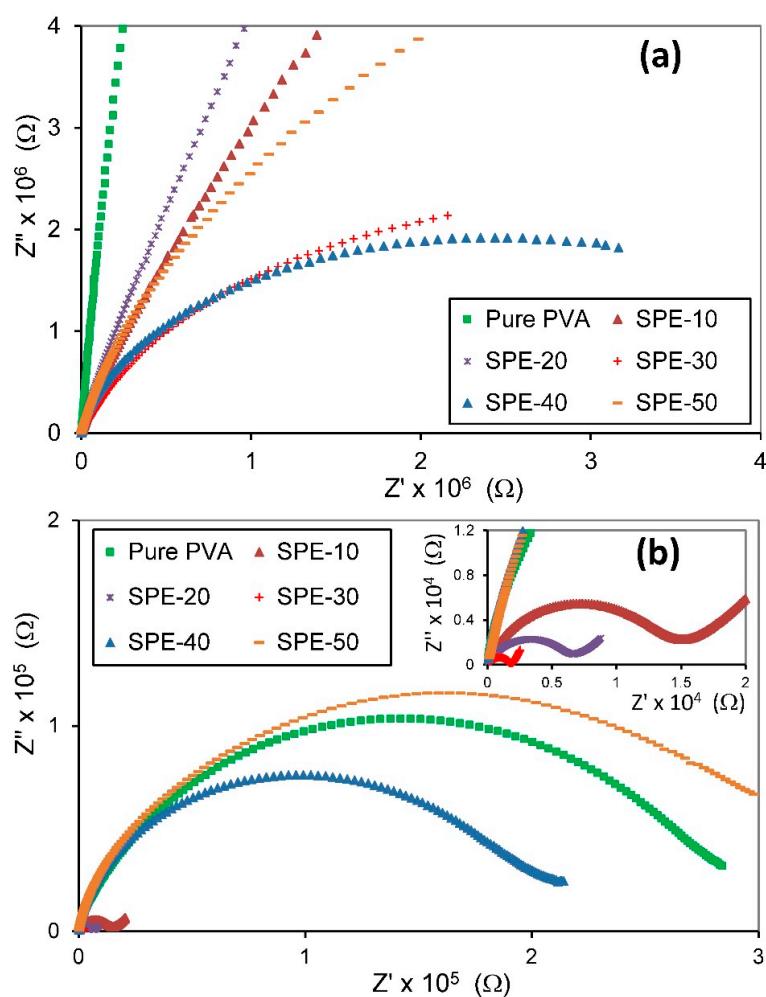

Figure 4. Cole-Cole plots for pure PVA and PVA/NH$_4$NO$_3$ proton-conducting SPE films at temperatures (**a**) 303 and (**b**) 353 K.

It is evident from Figure 4 that the change in salt concentrations and temperature plays a role in affecting the complex impedance spectra. At room temperature (Figure 4a), the complex impedance spectra have the same form for all SPE samples. However, at high temperature (Figure 4b), across the high concentration of NH_4NO_3, both high-frequency semicircular arc and low-frequency tail is observed. It is also evident that all the curves exhibit a tendency to bend towards the abscissa, and the radius of the semicircular arcs decreases with increasing temperature, denoting the increase in conductivity value with increasing temperature. Similar trends have been observed by many researchers for various SPE systems [41,42].

3.3.2. Frequency-Dependent Conductivity

The study of electrical conductivity spectra for SPE systems at various temperatures provides us with significant information about the mechanisms of ionic conduction in the SPE materials [43]. The measured complex impedance of electrolyte was used to compute electrical conductivity ($\sigma(\omega)$), using [44]:

$$\sigma(\omega) = \frac{d}{A} \frac{Z'}{(Z'^2 + Z''^2)} \tag{2}$$

where d and A are the thickness and the cross-section area of the sample, $\omega = 2\pi f$ is the angular frequency. The spectra of $\sigma(\omega)$ for pure PVA and SPE-30 at various temperatures are presented in Figure 5. It is clearly seen that the spectra of pure PVA can be divided into a frequency-independent plateau region at low frequency, and a frequency-dependent dispersion region at high frequency. However, the conductivity spectra for SPE-30 can be divided into three regions; a low-frequency dispersion region, a frequency-independent plateau region in the mid-frequency region, and a high frequencies dispersion region. The low-frequency dispersion region is attributed to the space-charge accumulation at the electrode-specimen contact. The frequency-independent plateau region ascribed to the DC conductivity (σ_{DC}). The high-frequency conductivity dispersion region is expressed by Jonscher's empirical power law:

$$\sigma(\omega) = \sigma_{DC} + B\omega^S \tag{3}$$

where B is a pre-exponential factor, and S is the dimensionless power-law exponent, generally varies in the range $0 < S < 1$ [45]. It is well established that the relation between S and temperature can be used to define the type of ion conduction processes that occur in the SPE due to the hopping of charge carriers over potential barriers in the system [14].
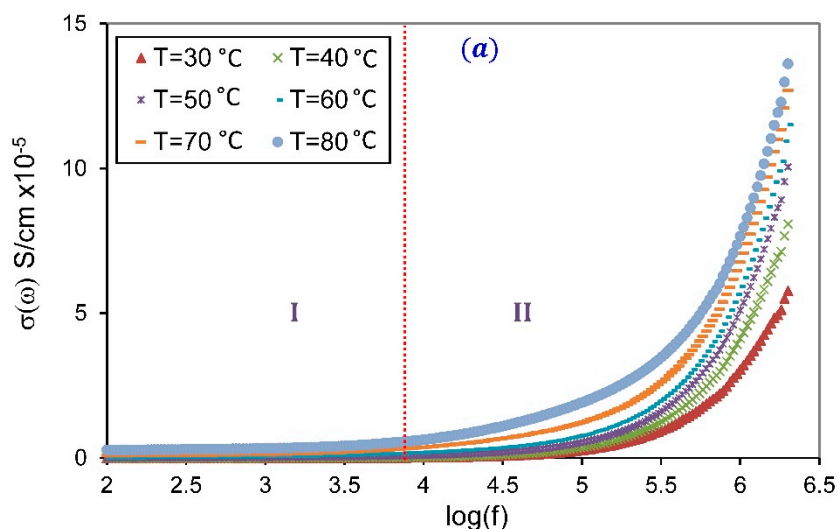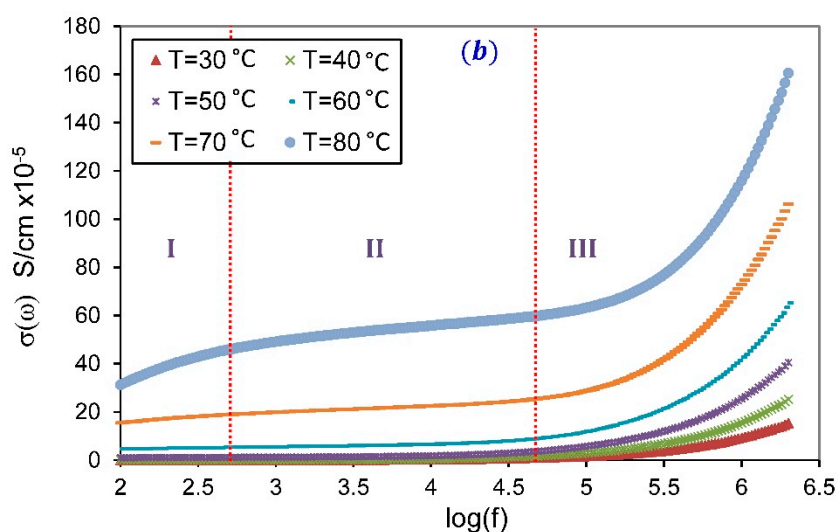

Figure 5. *Cont.*

Figure 5. Conductivity versus log(f) for (**a**) pure PVA, (**b**) SPE-30, at different temperatures.

The values of S were derived from the slope of the linear part of $\log \sigma(\omega)$ versus $\log \omega$ at higher frequencies region, as shown in Figure 6. In the present work, the acceptable frequency range is between $5.5 < \log \omega < 6.5$. The obtained values of S for pure PVA and PVA/NH$_4$NO$_3$ proton-conducting SPE films as a function of temperature are presented in Figure 7. For all presented samples, it is observed that the power-law exponent S decreases as temperature increases. It is also noted that the value of S is greater than unity at lower concentrations of NH$_4$NO$_3$ and low temperature, which suggests the occurrence of the 'nearly constant loss' phenomenon in these compositions. Generally, the nearly constant loss behavior in ionic conductors arises from the vibration of ions confined in the asymmetric double-well potential barrier, which correlated to the localized motions of charge carriers between neighboring sites rather than the hopping mechanisms in the conduction processes [46,47]. This phenomenon is observed for low-conducting SPEs at low temperatures, and cannot be observed when there are significant ion dynamics. Pal and Ghosh [48] have also reported the existence of a nearly constant loss at low temperatures in poly(methylmethacrylate)-lithium salt based polymer electrolytes plasticized with ethylene carbonate. They attribute the existence of this phenomenon to the cooperative hopping of charge carriers strongly coupled with the polymer chain dynamics.
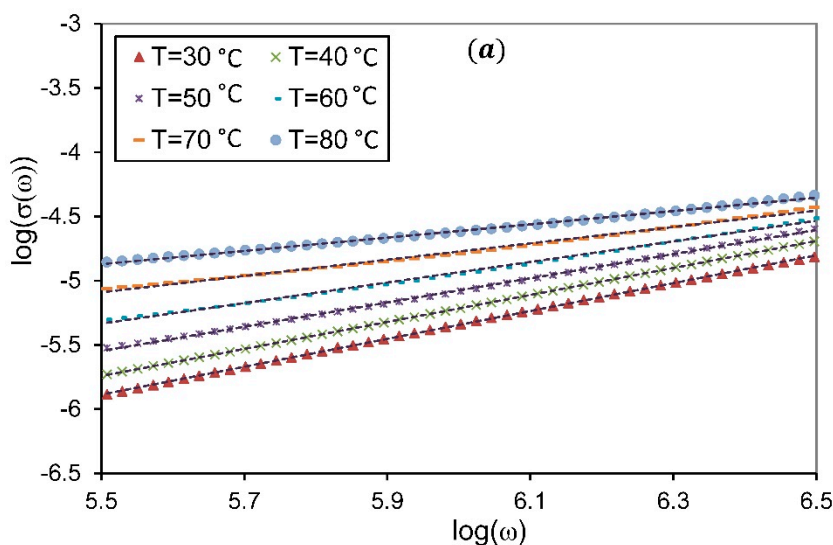

Figure 6. *Cont.*
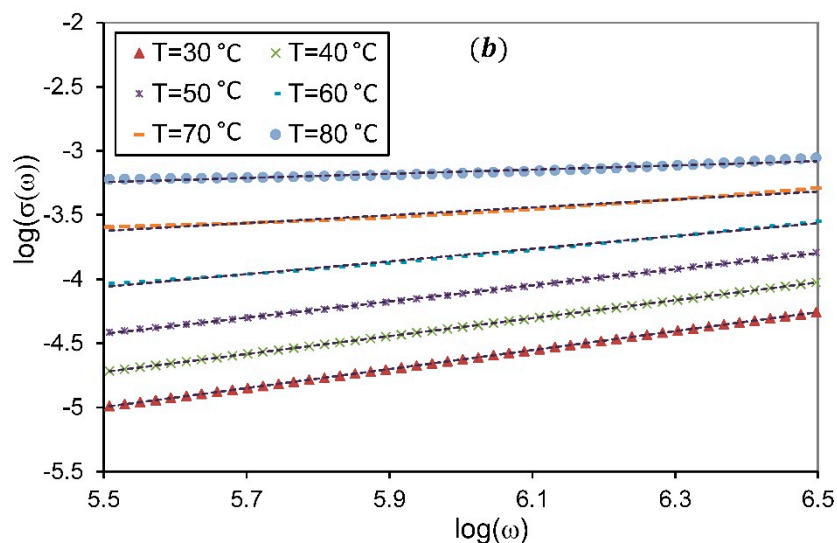
Figure 6. Plot of $\log \sigma(\omega)$ versus $\log \omega$ for (**a**) pure PVA, (**b**) SPE-30, at different temperatures.
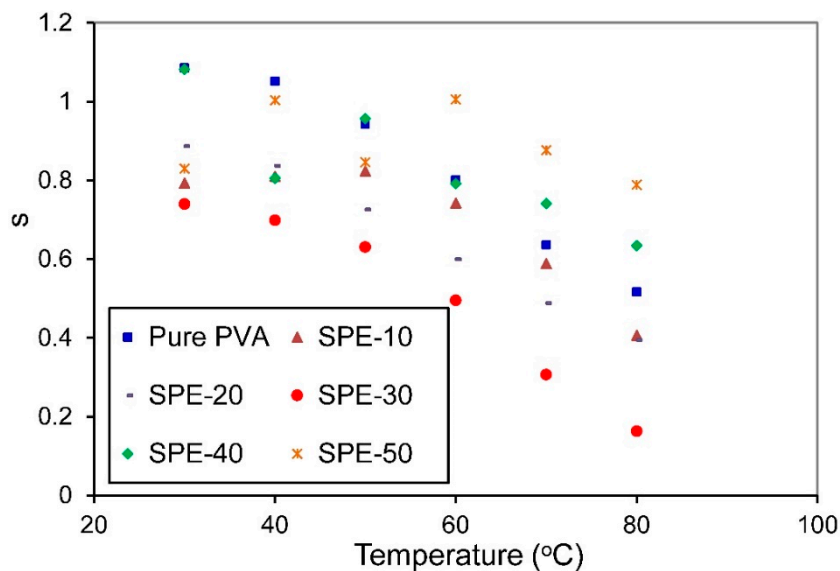

Figure 7. Variation of exponent S with temperature for PVA/NH$_4$NO$_3$ proton-conducting SPE films with different concentrations of NH$_4$NO$_3$.

Various theoretical models have been proposed to describe the conduction mechanism in electrolyte systems based on the variation of S with temperature. The most applicable models for SPEs are the correlated barrier hopping (CBH), the small polaron (SP), the overlapping large polaron (OLP), and the quantum mechanical tunneling (QMT) model [49]. According to the CBH model, S should decrease with increasing temperature, and the SP model is predominant if S increases with increasing the temperature. The OLP model is applicable if the S value decreases with increasing temperature to a minimum value and then increases again with further increases in temperature. Finally, the QMT model implies that S is temperature independent [7]. The continuous decrease in the S value with increasing temperature suggests that the CBH model is convenient to interpret the conduction mechanism in the present PVA/NH$_4$NO$_3$ proton-conducting SPE films, which means that the H$^+$ ions can drift by hopping between adjacent hydroxyl groups of the PVA (complexation sites) over the potential barrier separating them [50].

3.3.3. Bulk Conductivity

It is well reported that bulk conductivity (σ_{DC}) can be calculated by extrapolating the frequency-independent plateau region of electrical conductivity towards zero frequency [32,51]. Figure 8 deals with the bulk conductivity of the PVA/NH$_4$NO$_3$ proton-conducting SPE system heated at different temperatures. When the temperature increases, the bulk conductivity improved for all concentrations, indicating that the conductivity is thermally assisted. The continuous increase in σ_{DC} with increasing temperature for all compounds can be clarified based on the free-volume theory. As the temperature increase, the free-volume of the SPEs increase, causing the enhancement of the segmental motion of the chain, which facilitates the movement of ionic charge carriers [52].
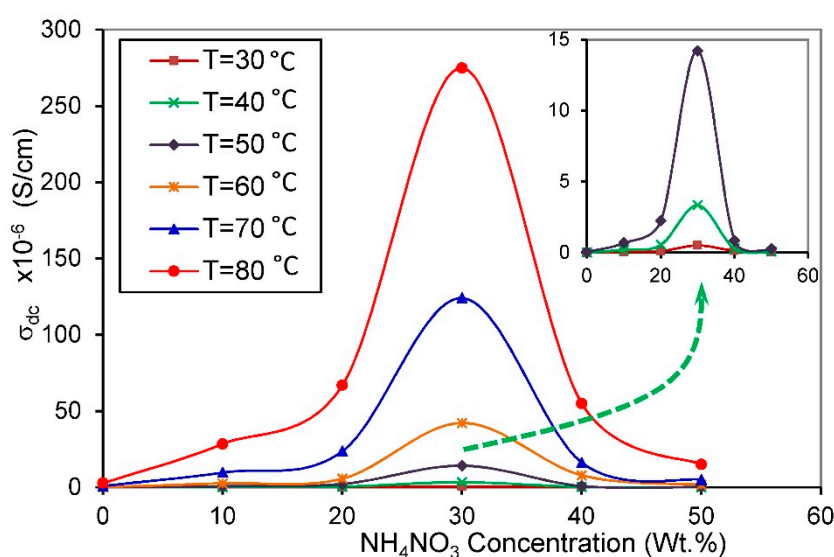

Figure 8. Conductance spectra for PVA/NH$_4$NO$_3$ proton-conducting SPE films with different salt concentrations at various temperatures.

The room temperature conductivity of pure PVA is 4×10^{-9} S/cm, which is compatible with the earlier reported value [53]. The electrical conductivity of SPE increased by several orders of magnitude with NH$_4$NO$_3$ loading. Among all SPE compositions, 30 wt.% of NH$_4$NO$_3$ doped polymer matrices show the maximum bulk conductivity in 5.17×10^{-5} S/cm at room temperature (303 K) and 2.74×10^{-4} S/cm at high temperature (353 K). This value is much higher than that achieved by Khandale et al. [54]; they observed maximum room temperature conductivity as 1.3×10^{-7} S/cm for PVA: ammonium acetate proton-conducting SPE.

The increment of NH$_4$NO$_3$ loading up to 30 wt.% caused an increase in the σ_{DC}, because of the rise in the number of free charge carriers (n) and their mobility (μ) since the DC conductivity is defined as the product of these two parameters, and the charge of the electron ($\sigma_{DC} = \sum en_i\mu_i$) [55]. The mobility of free ions in the SPE can be enhanced by increasing the amorphous fraction, which facilitates the movement of free ions by reducing the energy barrier prompting enhancement in the conductivity [32]. Recrystallization of the salt out of the film at high salt concentrations will contribute to reducing the number of mobile ions [56].

Above 30 wt.% of NH$_4$NO$_3$, the salt is no longer dissoluble within the matrix. This result is in concordance with XRD analysis, which demonstrates that no more of the salt can dissolve at a high concentration of NH$_4$NO$_3$.

From XRD results, the increase in electrical conductivity with increasing NH$_4$NO$_3$ content can be attributed to the reduction in the crystallinity phase of the host polymer matrix [57]. It is inferred that the SPE sample containing 30 wt.% of the salt is the most amorphous sample. The decreased trend in

the conductivity at higher salt concentrations is because of the increase in the degree of crystallinity, as verified by the XRD result in Figure 2.

3.3.4. Temperature-Dependent Conductivity

The temperature-dependent electrical conductivity may provide valuable information describing the ionic conduction behavior [55]. For all PVA/NH$_4$NO$_3$ proton-conducting SPE films, the conductivity increases exponentially with increasing the temperature due to the increase in the ion mobility. On the other hand, due to the complexity and the lack of correlation between the structure and transport properties of SPE systems, the ion transport in these systems cannot be comprehensively described [58]. Nevertheless, the temperature-dependent ionic conductivity of SPE was extensively studied using the experimentally Arrhenius and Vogel–Tammann–Fulcher (VTF) models [10].

The main factor influencing the ionic conductivity (σ) of SPE is the activation energy (E_A), because it corresponds to the energy barrier for ionic conduction. It was observed that E_A is inversely proportional to the conductivity of the system. The E_A is influenced by three factors, i.e., the nature of bonds, vacancies, and site geometry [59]. The value of E_A assesses the ionic mobility (μ) and charge carrier concentration (n). According to the Arrhenius equation, the activation energy (E_A) can be evaluated using the formula:

$$\sigma = \sigma_0 \exp\left(-\frac{E_A}{K_\beta T}\right) \tag{4}$$

where σ_0 is a pre-exponential factor, K_β is the Boltzmann constant, and T is the absolute temperature. The Arrhenius equation describes ionic transport as intermolecular ion hopping in a dilute electrolyte [60]. In most cases, a SPE is more suitably fitted by the VTF equation, which can be expressed as the following equation [61]:

$$\sigma = C/T^{1/2} \exp\left(-\frac{E_P}{K_\beta (T - T_0)}\right) \tag{5}$$

where C, E_P, T_0 are the constants determined through experimental data fitting. E_P is the pseudo-activation energy, and T_0 is the reference temperature, which is usually equal or lower than the glass transition temperature by 10–50 K. The VTF behavior is correlated with the transport of mobile ions and the movement of long-range polymer chain segments.

In this study, both Arrhenius and VTF equations are used to model the conductivity of the present PVA/NH$_4$NO$_3$ proton-conducting SPE films for the sake of verification of the validity of two models. The parameters in Arrhenius and VTF equations could be attained by linearizing the fitting Equations (4) and (5), which are tabulated in Table 2. T_0 was obtained by trial and error to make the conductivity-temperature data fit Equation (2). In this study T_0 is taken to be 140 K. The distinction in the conductivity as a component of inverse temperature for pure PVA and all PVA/NH$_4$NO$_3$ proton-conducting SPE films are displayed in Figure 9.

Table 2. Parameters determined through experimental data fitting using Arrhenius and Vogel–Tammann–Fulcher (VTF) models.

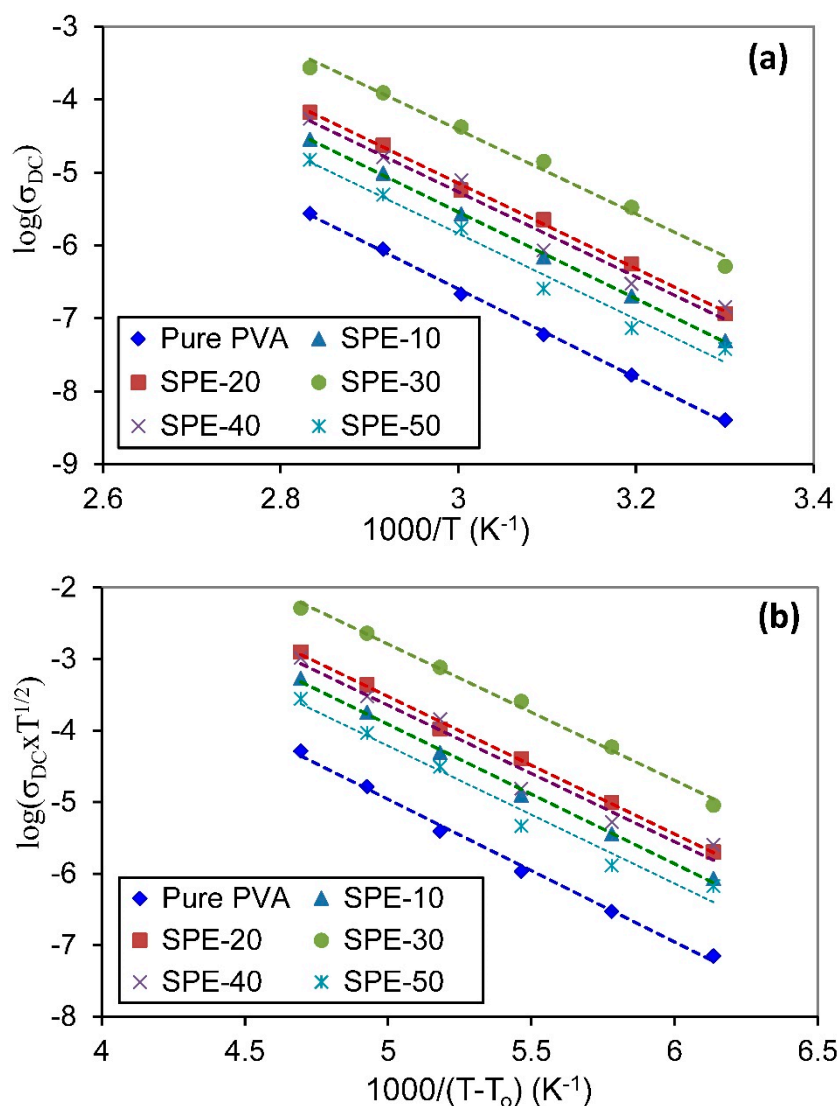| Samples	Arrhenius Model			VTF Model	
	E_A (*eV*)	R^2	T_0 (*K*)	E_P (*eV*)	R^2
Pure PVA	1.207	0.9988	140	0.396	0.9959
SPE-10	1.179	0.9994	140	0.387	0.9973
SPE-20	1.161	0.9977	140	0.382	0.9974
SPE-30	1.147	0.9896	140	0.378	0.9954
SPE-40	1.156	0.9811	140	0.379	0.9684
SPE-50	1.166	0.9808	140	0.382	0.9745

Figure 9. Temperature-dependence of DC conductivity for pure PVA and all PVA/NH$_4$NO$_3$ proton-conducting SPE films doped with various concentrations of NH$_4$NO$_3$, using (**a**) Arrhenius and (**b**) Vogel–Tammann–Fulcher (VTF) models.

The linear relationship of the σ_{DC} versus the reciprocal temperature indicates that the σ_{DC} increases exponentially with temperature, and the relaxation process is thermally activated [62]. The regression values (R^2) obtained for both models are close to unity, suggesting that all data points lie on the fitting straight lines. The values of activation energy (E_A) and pseudo-activation energy (E_P) were calculated from the slopes of the linear fits of Figure 9. The E_A represents the minimum energy required for charge carriers to hop from one site to another site through the material, thereby causing electrical conduction [63]. While, E_P is associated with the polymer segmental motion [55]. The values of E_A and E_P are least for the sample with the highest conductivity (SPE-30). Therefore, it can be concluded that the maximum conductivity of the SPE-30 sample was achieved by minimizing the energy barrier for ion migration.

4. Conclusions

A series of PVA/NH$_4$NO$_3$ proton-conducting SPE films were prepared by the solvent-casting process. The XRD patterns for SPEs confirm the reduction in the intensity of the peak corresponding to PVA upon an increase in the NH$_4$NO$_3$ content. The electrical conductivities were calculated,

and it was found to increase from order 10^{-9} S/cm to 10^{-5} S/cm at room temperature, and 10^{-4} S/cm at 353 K. The highest ionic conductivity at ambient temperature was achieved for PVA loaded 30 wt.% NH_4NO_3 which are associated with the decrease in free ions and lowest degree of crystallinity. The temperature-dependent AC conductivity analysis infers the dominance of the correlated barrier hopping (CBH) model in the conduction mechanism of the system. The increase in conductivity with temperature was studied using both the Arrhenius and VTF models. In both cases, the maximum conducting sample exhibits the lowest activation energy and pseudo-activation energy, respectively. This observation indicates that the polymer segmental motions play a crucial role in the ion transport processes in the present SPE system.

Author Contributions: O.G.A. supervised, conceived, and designed the experiments; M.A.M.S. performed the experiments; O.G.A. and M.A.M.S. analyzed data, wrote the initial manuscript, and approved the final version of the manuscript that was submitted. All authors have read and agreed to the published version of the manuscript.

Conflicts of Interest: The authors declare no conflict of interest.

References

1. Chandra, A.; Agrawal, R.C.; Mahipal, Y.K. Ion transport property studies on PEO-PVP blended solid polymer electrolyte membranes. *J. Phys. D Appl. Phys.* **2009**, *42*, 135107. [CrossRef]
2. Gadjourova, Z.; Andreev, Y.G.; Tunstall, D.P.; Bruce, P.G. Ionic conductivity in crystalline polymer electrolytes. *Nature* **2001**, *412*, 520–523. [CrossRef] [PubMed]
3. Salman, Y.A.K.; Abdullah, O.G.; Hanna, R.R.; Aziz, S.B. Conductivity and electrical properties of chitosan—Methylcellulose blend biopolymer electrolyte incorporated with lithium tetrafluoroborate. *Int. J. Electrochem. Sci.* **2018**, *13*, 3185–3199. [CrossRef]
4. Aziz, S.B.; Al-zangana, S.; Woo, H.J.; Kadir, M.F.Z.; Abdullah, O.G. The compatibility of chitosan with divalent salts over monovalent salts for the preparation of solid polymer electrolytes. *Results Phys.* **2018**, *11*, 826–836. [CrossRef]
5. Ahmed, H.T.; Abdullah, O.G. Preparation and composition optimization of PEO:MC polymer blend films to enhance electrical conductivity. *Polymers* **2019**, *11*, 853. [CrossRef]
6. Kumar, J.S.; Reddy, M.J.; Rao, U.V.S. Ion transport and battery studies of a new (PVP + KIO_3) polymer electrolyte system. *J. Mater. Sci.* **2006**, *41*, 6171–6173. [CrossRef]
7. Ahmed, H.T.; Jalal, V.J.; Tahir, D.A.; Mohamad, A.H.; Abdullah, O.G. Effect of PEG as a plasticizer on the electrical and optical properties of polymer blend electrolyte $MC-CH-LiBF_4$ based films. *Results Phys.* **2019**, *15*, 102735. [CrossRef]
8. Hemalatha, R.; Alagar, M.; Selvasekarapandian, S.; Sundaresan, B.; Moniha, V.; Boopath, G.; Selvin, P.C. Preparation and characterization of proton-conducting polymer electrolyte based on PVA, amino acid proline, and NH_4Cl and its applications to electrochemical device. *Ionics* **2019**, *25*, 141–154. [CrossRef]
9. Patra, S.; Puthirath, A.B.; Vineesh, T.V.; Narayanaru, S.; Soman, B.; Suriyakumar, S.; Stephan, A.M.; Narayanan, T.N. On the development of a proton conducting solid polymer electrolyte using poly (ethylene oxide). *Sustain. Energy Fuels* **2018**, *2*, 1870–1877. [CrossRef]
10. Ahmed, H.T.; Abdullah, O.G. Structural and ionic conductivity characterization of PEO:MC-NH_4I proton-conducting polymer blend electrolytes based films. *Results Phys.* **2020**, *16*, 102861. [CrossRef]
11. Ramya, C.S.; Selvasekarapandian, S.; Hirankumar, G.; Savitha, T.; Angelo, P.C. Investigation on dielectric relaxations of PVP-NH_4SCN polymer electrolyte. *J. Non-Cryst. Solids* **2008**, *354*, 1494–1502. [CrossRef]
12. Agrawal, S.L.; Singh, M.; Tripathi, M.; Dwivedi, M.M.; Pandey, K. Dielectric relaxation studies on [PEO-SiO_2]:NH_4SCN nanocomposite polymer electrolyte films. *J. Mater. Sci.* **2009**, *44*, 6060–6068. [CrossRef]
13. Borah, P.; Dutta, A. Conductivity study of some polymer electrolytes based on polyacrylonitrile. *Ionics* **2009**, *15*, 711–716. [CrossRef]
14. Abdullah, O.G.; Saleem, S.A. Effect of copper sulfide nanoparticles on the optical and electrical behavior of poly (vinyl alcohol) films. *J. Electron. Mater.* **2016**, *45*, 5910–5920. [CrossRef]

15. Aziz, S.B.; Abdullah, O.G.; Rasheed, M.A. Structural and electrical characteristics of PVA:NaTf based solid polymer electrolytes: Role of lattice energy of salts on electrical DC conductivity. *J. Mater. Sci. Mater. Electron.* **2017**, *28*, 12873–12884. [CrossRef]

16. Abdullah, O.G.; Aziz, S.B.; Rasheed, M.A. Incorporation of NH_4NO_3 into MC-PVA blend-based polymer to prepare proton-conducting polymer electrolyte films. *Ionics* **2018**, *24*, 777–785. [CrossRef]

17. Radha, K.P.; Selvasekarapandian, S.; Karthikeyan, S.; Hema, M.; Sanjeeviraja, C. Synthesis and impedance analysis of proton-conducting polymer electrolyte PVA:NH_4F. *Ionics* **2013**, *19*, 1437–1447. [CrossRef]

18. Hema, M.; Selvasekarapandian, S.; Arunkumar, D.; Sakunthala, A.; Nithya, H. FTIR, XRD and AC impedance spectroscopic study on PVA based polymer electrolyte doped with NH_4X (X = Cl, Br, I). *J. Non-Cryst. Solids* **2009**, *355*, 84–90. [CrossRef]

19. Aziz, S.B.; Abdullah, O.G.; Hussein, S.A.; Ahmed, H.M. Effect of PVA blending on structural and ion transport properties of CS:AgNt based polymer electrolyte membrane. *Polymers* **2017**, *9*, 622. [CrossRef]

20. Abdullah, O.G. Synthesis of single-phase zinc chromite nano-spinel embedded in polyvinyl alcohol films and its effects on energy band gap. *J. Mater. Sci. Mater. Electron.* **2016**, *27*, 12106–12111. [CrossRef]

21. Bdewi, S.F.; Abdullah, O.G.; Aziz, B.K.; Mutar, A.A.R. Synthesis, structural and optical characterization of MgO nanocrystalline embedded in PVA matrix. *J. Inorg. Organomet. Polym. Mater.* **2016**, *26*, 326–334. [CrossRef]

22. Zagorskaya, S.A.; Tretinnikov, O.N. Infrared spectra and structure of solid polymer electrolytes based on poly (vinyl alcohol) and lithium halides. *Polym. Sci. Ser. A* **2019**, *61*, 514–519. [CrossRef]

23. Abdullah, O.G.; Salman, Y.A.K.; Saleem, S.A. Electrical conductivity and dielectric characteristics of in-situ prepared PVA/HgS nanocomposite films. *J. Mater. Sci. Mater. Electron.* **2016**, *27*, 3591–3598. [CrossRef]

24. Moniha, V.; Alagar, M.; Selvasekarapandian, S.; Sundaresan, B.; Boopathi, G. Conductive bio-polymer electrolyte iota-carrageenan with ammonium nitrate for application in electrochemical devices. *J. Non-Cryst. Solids* **2018**, *481*, 424–434. [CrossRef]

25. Shuhaimi, N.E.A.; Teo, L.P.; Majid, S.R.; Arof, A.K. Transport studies of NH_4NO_3 doped methyl cellulose electrolyte. *Synth. Met.* **2010**, *160*, 1040–1044. [CrossRef]

26. Mohamad, A.H.; Saeed, S.R.; Abdullah, O.G. Synthesis of very-fine PbS nanoparticles dispersed homogeneously in MC matrix: Effect of concentration on the structural and optical properties of the host polymer. *Mater. Res. Express* **2019**, *6*, 115332. [CrossRef]

27. Abdullah, O.G.; Aziz, S.B.; Rasheed, M.A. Structural and optical characterization of PVA:$KMnO_4$ based solid polymer electrolyte. *Results Phys.* **2016**, *6*, 1103–1108. [CrossRef]

28. Zainuddin, N.K.; Samsudin, A.S. Investigation on the effect of NH_4Br at transport properties in K–Carrageenan based biopolymer electrolytes via structural and electrical analysis. *Mater. Today Commun.* **2018**, *14*, 199–209. [CrossRef]

29. Aziz, S.B.; Abdullah, O.G.; Rasheed, M.A.; Ahmed, H.M. Effect of high salt concentration (HSC) on structural, morphological and electrical characteristics of chitosan based solid polymer electrolytes. *Polymers* **2017**, *9*, 187. [CrossRef]

30. Wojdyr, M. Fityk: A general-purpose peak fitting program. *J. Appl. Crystallogr.* **2010**, *43*, 1126–1128. [CrossRef]

31. Rajendran, S.; Sivakumar, P. An investigation of PVdF/PVC-based blend electrolytes with EC/PC as plasticizers in lithium battery applications. *Physica B* **2008**, *403*, 509–516. [CrossRef]

32. Abdullah, O.G.; Hanna, R.R.; Salman, Y.A.K. Structural and electrical conductivity of CH:MC bio-poly-blend films: Optimize the perfect composition of the blend system. *Bull. Mater. Sci.* **2019**, *42*, 64. [CrossRef]

33. Kadir, M.F.Z.; Majid, S.R.; Arof, A.K. Plasticized chitosan-PVA blend polymer electrolyte based proton battery. *Electrochim. Acta* **2010**, *55*, 1475–1482. [CrossRef]

34. Patla, S.K.; Ray, R.; Asokan, K.; Karmakar, S. Investigation of ionic conduction in PEO-PVDF based blend polymer electrolytes. *J. Appl. Phys.* **2018**, *123*, 125102. [CrossRef]

35. Kadir, M.F.Z.; Aspanut, Z.; Yahya, R.; Arof, A.K. Chitosan–PEO proton conducting polymer electrolyte membrane doped with NH_4NO_3. *Mater. Res. Innov.* **2011**, *15*, s164–s167. [CrossRef]

36. Mobarak, N.N.; Ahmad, A.; Abdullah, M.P.; Ramli, N.; Rahman, M.Y.A. Conductivity enhancement via chemical modification of chitosan based green polymer electrolyte. *Electrochim. Acta* **2013**, *92*, 161–167. [CrossRef]

37. Naiwi, T.S.R.T.; Aung, M.M.; Ahmad, A.; Rayung, M.; Suait, M.S.; Yusof, N.A.; Lae, K.Z.W. Enhancement of plasticizing effect on bio-based polyurethane acrylate solid polymer electrolyte and its properties. *Polymers* **2018**, *10*, 1142. [CrossRef]

38. Chai, M.N.; Isa, M.I.N. Electrical characterization and ionic transport properties of carboxyl methylcellulose-oleic acid solid polymer electrolytes. *Int. J. Polym. Anal. Charact.* **2013**, *18*, 280–286. [CrossRef]

39. Ramesh, S.; Arof, A.K. Ionic conductivity studies of plasticized poly (vinyl chloride) polymer electrolytes. *Mater. Sci. Eng. B* **2001**, *85*, 10–15. [CrossRef]

40. Mohamad, A.H.; Abdullah, O.G.; Saeed, S.R. Effect of very fine nanoparticle and temperature on the electric and dielectric properties of MC-PbS polymer nanocomposite films. *Results Phys.* **2020**, *16*, 102898. [CrossRef]

41. Hema, M.; Selvasekerapandian, S.; Sakunthala, A.; Arunkumar, D.; Nithya, H. Structural, vibrational and electrical characterization of PVA-NH$_4$Br polymer electrolyte system. *Physica B* **2008**, *403*, 2740–2747. [CrossRef]

42. Ravi, M.; Pavani, Y.; Kumar, K.K.; Bhavani, S.; Sharma, A.K.; Rao, V.V.R.N. Studies on electrical and dielectric properties of PVP:KBrO$_4$ complexed polymer electrolyte films. *Mater. Chem. Phys.* **2011**, *130*, 442–448. [CrossRef]

43. Karan, N.K.; Pradhan, D.K.; Thomas, R.; Natesan, B.; Katiyar, R.S. Solid polymer electrolytes based on polyethylene oxide and lithium trifluoro-methane sulfonate (PEO-LiCF$_3$SO$_3$): Ionic conductivity and dielectric relaxation. *Solid State Ion.* **2008**, *179*, 689–696. [CrossRef]

44. Bandara, T.M.W.J.; DeSilva, L.A.; Gunasekara, L.B.E.; Dehipawala, S.; Mellander, B.E. Determination of charge carrier transport parameters in a polymer electrolyte intended for Li-ion batteries using electrochemical impedance analysis. *J. Solid State Electr.* **2020**, *24*, 1207–1216. [CrossRef]

45. Rosli, N.H.A.; Chan, C.H.; Subban, R.H.Y.; Winie, T. Studies on the structural and electrical properties of hexanoyl chitosan/polystyrene-based polymer electrolytes. *Phys. Procedia* **2012**, *25*, 215–220. [CrossRef]

46. Funke, K.; Singh, P.; Banhatti, R.D. Conductivity dispersion in supercooled calcium potassium nitrate: Caged ionic motion viewed as part of standard behaviour. *Phys. Chem. Chem. Phys.* **2007**, *9*, 5582–5590. [CrossRef]

47. Chaurasia, S.K.; Saroj, A.L.; Shalu; Singh, V.K.; Tripathi, A.K.; Gupta, A.K.; Verma, Y.L.; Singh, R.K. Studies on structural, thermal and AC conductivity scaling of PEO-LiPF$_6$ polymer electrolyte with added ionic liquid [BMIMPF$_6$]. *AIP Adv.* **2015**, *5*, 077178. [CrossRef]

48. Pal, P.; Ghosh, A. Dielectric spectroscopy of PMMA-LiClO$_4$ based polymer electrolyte plasticized with ethylene carbonate EC. *J. Appl. Phys.* **2016**, *120*, 045108. [CrossRef]

49. Aziz, S.B.; Abdullah, O.G.; Saeed, S.R.; Ahmed, H.M. Electrical and dielectric properties of copper ion conducting solid polymer electrolytes based on chitosan: CBH model for ion transport mechanism. *Int. J. Electrochem. Sci.* **2018**, *13*, 3812–3826. [CrossRef]

50. Abdullah, O.G.; Aziz, S.B.; Saber, D.R. Characterizations of pure and Pb^{2+} ion doped methylcellulose based biopolymer electrolyte films: Optical and electrical properties. *Int. J. Electrochem. Sci.* **2018**, *13*, 11931–11952. [CrossRef]

51. Abdullah, O.G.; Hanna, R.R.; Salman, Y.A.K. Structural, optical, and electrical characterization of chitosan: Methylcellulose polymer blends based film. *J. Mater. Sci. Mater. Electron.* **2017**, *28*, 10283–10294. [CrossRef]

52. Parameswaran, V.; Nallamuthu, N.; Devendran, P.; Nagarajan, E.R.; Manikandan, A. Electrical conductivity studies on ammonium bromide incorporated with Zwitterionic polymer blend electrolyte for battery application. *Physica B* **2017**, *515*, 89–98. [CrossRef]

53. Sengwa, R.J.; Choudhary, S. Investigation of correlation between dielectric parameters and nanostructures in aqueous solution grown poly (vinyl alcohol)-montmorillonite clay nanocomposites by dielectric relaxation spectroscopy. *Express Polym. Lett.* **2010**, *4*, 559–569. [CrossRef]

54. Khandale, A.P.; Bhoga, S.S.; Gedam, S.K. Study on ammonium acetate salt-added polyvinyl alcohol-based solid proton-conducting polymer electrolytes. *Ionics* **2013**, *19*, 1619–1626. [CrossRef]

55. Gohel, K.; Kanchan, D.K. Effect of PC:DEC plasticizers on structural and electrical properties of PVDF-HFP:PMMA based gel polymer electrolyte system. *J. Mater. Sci. Mater. Electron.* **2019**, *30*, 12260–12268. [CrossRef]

56. Ahmed, H.T.; Abdullah, O.G. Impedance and ionic transport properties of proton-conducting electrolytes based on polyethylene oxide/methylcellulose blend polymers. *J. Sci. Adv. Mater. Devices* **2020**, *5*, 125–133. [CrossRef]

57. Yusof, Y.M.; Shukur, M.F.; Illias, H.A.; Kadir, M.F.Z. Conductivity and electrical properties of corn starch-chitosan blend biopolymer electrolyte incorporated with ammonium iodide. *Phys. Scr.* **2014**, *89*, 035701. [CrossRef]

58. Sundaramahalingam, K.; Vanitha, D.; Nallamuthu, N.; Manikandan, A.; Muthuvinayagam, M. Electrical properties of lithium bromide poly ethylene oxide/poly vinyl pyrrolidone polymer blend electrolyte. *Physica B* **2019**, *553*, 120–126. [CrossRef]

59. Sahu, G.; Rangasamy, E.; Li, J.; Chen, Y.; An, K.; Dudney, N.; Liang, C. A high-conduction Ge substituted Li3AsS4 solid electrolyte with exceptional low activation energy. *J. Mater. Chem. A* **2014**, *2*, 10396–10403. [CrossRef]

60. Idris, N.H.; Majid, S.R.; Khiar, A.S.A.; Hassan, M.F.; Arof, A.K. Conductivity studies on chitosan/PEO blends with LiTFSI salt. *Ionics* **2005**, *11*, 375–377. [CrossRef]

61. Hamsan, M.H.; Shukur, M.F.; Kadir, M.F.Z. NH_4NO_3 as charge carrier contributor in glycerolized potato starch-methyl cellulose blend-based polymer electrolyte and the application in electrochemical double-layer capacitor. *Ionics* **2017**, *23*, 3429–3453. [CrossRef]

62. Vijaya, N.; Selvasekarapandian, S.; Hirankumar, G.; Karthikeyan, S.; Nithya, H.; Ramya, C.S.; Prabu, M. Structural, vibrational, thermal, and conductivity studies on proton-conducting polymer electrolyte based on poly (N-vinylpyrrolidone). *Ionics* **2012**, *18*, 91–99. [CrossRef]

63. Buraidah, M.H.; Teo, L.P.; Majid, S.R.; Arof, A.K. Ionic conductivity by correlated barrier hopping in NH_4I doped chitosan solid electrolyte. *Physica B* **2009**, *404*, 1373–1379. [CrossRef]